Studies on Preparation and Electrical Properties of Rare Earth Sulfides

(希土類硫化物の合成とその電気的性質に関する研究)

1981

MINEO SATO

Department of Applied Chemistry

Faculty of engineering

Osaka University

Preface

The work in this thesis was performed under the guidance by Professor Jiro Shiokawa at the Department of Applied Chemistry, Faculty of Engineering, Osaka University.

The object of this thesis is to prepare various metal sulfides involving rare earth ions and to study their physical properties, especially electrical transport properties. The author hopes that the work described in this thesis gives many fundamental data on developing new semiconducting materials.

Mineo Sato

Suita, Osaka

January, 1981

Contents

General introduction

Since the individual rare earths became available in high purity and at fairly moderate cost, developments have been directed more toward utilization of their distinctive properties. These are primarily optical, magnetic, and nuclear properties. These properties of rare earths, as a whole, change only gradually on going lanthanum to lutetium and are almost identical so far as the ions are in the normal trivalent state. However, when they are in a valence state other than the trivalent state, unusual properties come into existence owing to variable valences. For example, samarium, europium, and ytterbium exhibit a divalent state as well as a trivalent state. Undoubtedly, this is due to the enhanced stability of half filled and completely filled 4f shells. Divalent state is easily stabilized by the low electronegativity of the anions. In this viewpoint, the divalent state of these elements is more stable in sulfides than in oxides.

In general, rare earth sulfides can be approximately divided into two groups on the basis of their crystal structures in which interesting physical properties are often observed. One is rock salt-type rare earth monosulfides denoted by LnS (Ln = rare earths). Another is a series of Th_3P_4-type rare earth sulfides, $Ln_{3-x}S_4$. Since one electron in the 5d orbital of rare earth ions in monosulfides does not take part in the bonding with sulfur anions, the 5d orbitals overlap one another to give a partially filled band which contains one electron per cation, resulting in metallic conduction. The 4f electrons are

localized and they determine the magnetic properties. The divalent samarium, europium, and ytterbium ions are, however, exceptional; they have configurations $4f^6$, $4f^7$, and $4f^{14}$ respectively, without 5d electrons. As a result, SmS, EuS, and YbS resemble alkaline earth sulfides rather than LnS; they are non-metallic and the lattice parameter is not shortened by conduction electrons. Particularly, SmS and EuS exhibit extremely unusual physical behaviors because of the unique properties of divalent samarium and europium ions. It has been observed for SmS that the valence or electronic occupation of the 4f shell of samarium atom may change discontinuously with increasing temperature and external pressure. This valence change causes large changes in the electrical resistivity, crystal volume, optical reflectivity, and magnetic properties. These phenomena have not only a theoretical interest but also practical applications as electronic switching or memory devices [1]. Europium monosulfide, which is ferromagnetic with a Curie temperature of 16K, has been highlighted as a new magnetic semiconductor. The optical measurements show that this material remains a semiconductor also below its magnetic ordering temperature and that it also exhibits a new magneto-optical phenomenon, namely the red shift of the absorption edge of a ferromagnetic semiconductor upon cooling below T_c [2].

On the other hand, rare earth sulfides with the Th_3P_4 structure, which are denoted by $Ln_{3-x}S_4$, have the great versatility of this phase in accommodating large quantities of metal site vacancies and cation substitutions. The composition generally varies between Ln_2S_3 and Ln_3S_4. The sulfide, Ln_2S_3,

in the Th_3P_4 structure is insulating or semiconducting and corresponds to a vacancy concentration of 1/9 of metal sites. When the vacancies are filled with trivalent metal ions, the sulfide, Ln_3S_4, is metallic and demonstrates almost the same lattice parameter as that of Ln_2S_3. Thus, the versatility of this structure to accommodate a variety of substitutions and hence various electron/atom is expected to encourage not only many phase studies but also studies involving electrical transport phenomena.

From the above point of view, it is interesting to study the electrical transport properties of the Th_3P_4-type rare earth sulfides including divalent samarium and europium ions which exhibit unusual magnetic, optical, and other physical behaviors among other rare earth ions. Also, such a study is expected to give many fundamental data on developing new semiconducting devices such as rectifiers, photocells, thermistors, and detectors, which have become an important part of modern electronics.

The present work has been undertaken for the purposes mentioned above, and is composed of three chapters and concluding remarks.

Chapter 1 describes electrical properties of the Th_3P_4-type rare earth sulfides $EuLn_2S_4$ (Ln = La - Gd). In this chapter, electrical properties of $EuLn_2S_4$ have been discussed with the aid of bond characters in the crystals and the stoichiometry of compositions. Chapter 2 describes electrical and magnetic properties of mixed valence rare earth sulfides, $(Sm_{1-x}Gd_x)_3S_4$. In this chapter, electrical properties of $(Sm_{1-x}Gd_x)_3S_4$ have

been studied on the basis of the valence transition of samarium ions. Chapter 3 describes electrical transport behaviors of ferromagnetic $Gd_{3-x}S_4$ near its Curie temperature. In this chapter, a magnetoresistive effect of $Gd_{3-x}S_4$ has been discussed with a proposed model.

Most results of the investigation in this thesis have already been published in the following five papers.

1. Electrical Conductivity of Th_3P_4-Type $EuLn_2S_4$.
   Mineo Sato, Gin-ya Adachi, and Jiro Shiokawa,
   J. Solid State Chem., 31, 337(1980).
2. Electrical Transport Properties of a Nonstoichiometric Rare Earth Sulfide, $EuGd_2S_4$.
   Mineo Sato, Gin-ya Adachi, and Jiro Shiokawa,
   J. Solid State Chem., 33, 277(1980).
3. Electrical Properties of Mixed Valence Rare Earth Sulfides, $(Sm_{1-x}Gd_x)_3S_4$.
   Mineo Sato, Gin-ya Adachi, and Jiro Shiokawa,
   Solid State Comm., 34, 69(1980).
4. Electrical Properties of Ferromagnetic $Gd_{3-x}S_4$ near its Curie temperature.
   Mineo Sato, Ken-ichi Niki, Gin-ya Adachi, and Jiro Shiokawa,
   Mat. Res. Bull., 15, 995(1980).
5. Electrical and Magnetic Properties of Rare Earth Sulfides, $(Sm_{1-x}Gd_x)_3S_4$.
   Mineo Sato, Gin-ya Adachi, Ken-ichi Niki, and Jiro Shiokawa,
   J. Solid State Chem., in contribution.

Chapter 1

Electrical Transport Properties of Stoichiometric and Nonstoichiometric Th_3P_4-Type Rare Earth Sulfides, $EuLn_2S_4$ (Ln = La - Gd)

1-1 Introduction

The rare earth sulfides with the Th_3P_4 structure, which can be described by the formula $Ln_{3-x}S_4$, are of interest because they exhibit a wide range of electrical and magnetic properties without changing crystal structure [3-7]. The Th_3P_4 structure belongs to the space group $I\bar{4}3d$-T_d^6, which is a body-centered cubic structure with four formula units in an unit cell [8,9].

Figure 1(a) shows the coordination polyhedra of anions in the structure. A cation is surrounded by eight anion and cation nearest neighbors, which form the vertices of an irregular polyhedron, respectively. As is shown in Fig. 1(b), a 4-fold rotatory reflection axis exists per one cation site and

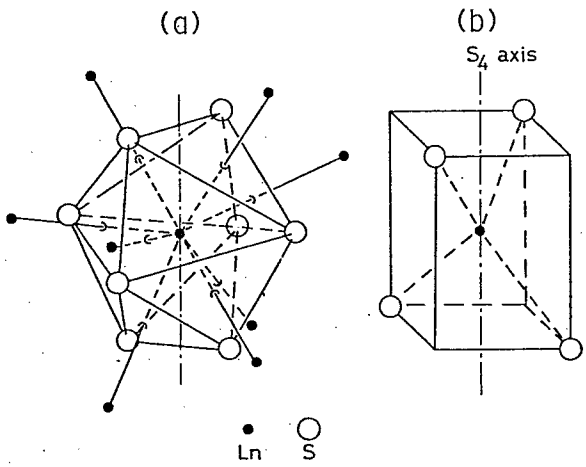

Fig. 1. Coordination polyhedra of anions in cubic Th_3P_4 (space group $I\bar{4}3d$-T_d^6) rare earth sulfides, (a), and 4-fold rotatory axis on a cation site, (b).

the axis is at right angles to two other 4-fold rotatory axes.

These $Ln_{3-x}S_4$ rare earth sulfides may be described by the formula $(Ln^{3+})_{3-x}V_x(S^{2-})_4(e^-)_{1-3x}$, where the vacancies designated by V are on the rare earth sites, and if x=1/3 and x=0, stoichiometric compounds Ln_2S_3 and Ln_3S_4, respectively, are formed [10]. The number of the conduction electrons and the average magnetic moments in these compounds can be varied continuously over wide ranges by substitution of metal ions with different valences or by variation of the metal/sulfur ratio [11]. The vacancies present in the Ln_2S_3 can be accommodated by a large number of additional metal ions without changing the crystal structure. This fact leads to many interesting changes in the electrical and the magnetic properties of these compounds. Cutler and his co-workers [4,10,12] had studied in detail the electrical transport properties of $Ce_{3-x}S_4$. They observed a transition from a metal (Ce_3S_4) to an insulator (Ce_2S_3) type of transport and suggested that the conduction electrons occupied a partially filled 5d band for Ce_3S_4. On the other hand, it is known that rare earth sulfides $LnLn'_2S_4$ (Ln = Sm, Eu, Yb, and Ln' = La - Gd) prepared by the solid state reaction between LnS and Ln'_2S_3 have the Th_3P_4-type crystal structure [13]. Also, Lugscheider et al. [14] have recently reported that $EuLn_2S_4$ was antiferromagnetic at low temperature. These compounds should be insulators if they are stoichiometric, since Eu ion in these compounds is divalent and Ln ion trivalent as shown from the magnetic susceptibility measurements. In practice, the physical properties of $EuLn_2S_4$ seem to be affected by their stoichiometry because they have the Th_3P_4 structure

which is stable over a wide composition range.

The aim of this chapter is to investigate the dependence of temperature and sulfur vapor pressure on the electrical conductivity of $EuLn_2S_4$, and also to discuss the influence of nonstoichiometry on the electrical transport phenomena of them.

1-2 Experimental

Preparation of samples

Stoichiometric $EuLn_2S_4$ samples were prepared by the solid state reaction between EuS and Ln_2S_3 (Ln = La - Gd). First, EuS and Ln_2S_3 were respectively obtained by sulfurizing the corresponding rare earth chlorides in a dried H_2S stream (100 ml/min) at 900 to 1100°C for 5 hr. For the preparation of $EuLn_2S_4$, starting mixtures with the appropriate molecular ratio of EuS and Ln_2S_3 were ground together in an agate motar and pressed into pellets at 200 kg/cm^2. The pellets were put in a graphite crucible in a quartz tube and were sintered in a dried H_2S stream (100 ml/min) at 1000°C for 3 hr. In order to obtain nonstoichiometric $EuGd_2S_4$ samples, stoichiometric $EuGd_2S_4$ was heated on a molybdenum plate in an induction furnace at various temperatures (1500 - 1800°C) for 3 hr under vacuum ($\sim 10^{-4}$ mmHg).

Analyses

The atomic ratio (Eu : Gd) in the nonstoichiometric $EuGd_2S_4$ samples was determined with a Rigaku Denki X-ray fluorescent spectrometer equipped with a Si(Li) detector. The quantity of sulfur was determined by the conventional wet chemical analysis,

sulfur anion in the sample being oxidized into SO_4^{2-} anion by CCl_4 + Br_2 (2 : 1) solution and concentrated HNO_3. The content of sulfur was obtained as the weight of $BaSO_4$.

X-ray diffraction technique

The phase purity and structure type of the resulting materials were characterized by X-ray powder data from a Rigaku Denki "Rota-flex" diffractometer with a scintillation detector and CuK_α radiation (λ=1.5418 Å). The lattice parameters were refined by the least squares method for unambigously indexed reflections.

Magnetic susceptibility measurements

The magnetic susceptibility data of the resulting materials were obtained with a Shimadzu MB-11 magnetic balance in the temperature range 77 - 300K.

Electrical conductivity measurements

The electrical conductivity measurements were carried out by applying the dc two-probe method with a polycrystalline sintered pellet in an atmosphere of He (at about 1 atm) or sulfur vapor under various pressures. For measurements in He, the electrical conductivities of the samples were measured as a function of temperature over a temperature range 77 - 770K. A very thin layer of Au was evaporated on pellet end faces, which were put in contact with Ag electrodes. From the measurements of current-voltage characteristics, the contact between the sample and the electrode was found to be ohmic at both room temperature and 77K. The data obtained were calibrated with those obtained by the dc four-probe method at room temperature. For the measurements in sulfur vapor, the dependence of sulfur

pressure on conductivity was investigated. In these measurements, a thin layer of Au was also deposited on the pellet end faces and the pellet was held between two Pt plate electrodes supported by Pyrex glass plates.

Thermoelectric power measurements

Thermoelectric power measurements were carried out with an apparatus as shown in Fig. 2. The sample used for this measurement was bar-shaped and was held in place between two copper blocks. Thin layers of silver paste were applied to the copper/sample interface so that an excellent ohmic contact was obtained. Temperature gradients were imposed by controlling the amount of power in heating elements wound on the copper blocks and were always less than 5°C. The thermoelectric power, S, was measured as a function of temperature over the range 120 - 400K and whether the material was n-type or p-type, was judged by the sign of S.

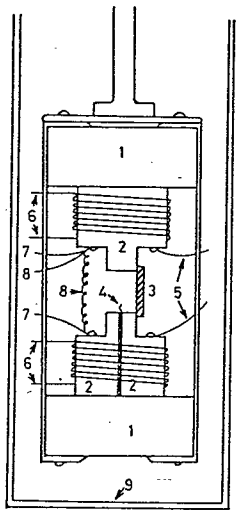

1 Teflon block
2 Copper block
3 Sample
4 Teflon sheet
5 Copper lead
6 Manganin heating element
7 Thermocouple (copper)
8 Thermocouple (constantan)
9 Copper

Fig. 2. Apparatus for thermoelectric power measurements.

1-3 Results and discussion

a) Stoichiometric rare earth sulfides $EuLn_2S_4$

X-ray diffraction measurements of the sintered $EuLn_2S_4$ (Ln = La ~ Gd) have shown only the pattern expected for the Th_3P_4 structure (space group $I\bar{4}3d$-T_d^6). Magnetic susceptibility measurements were performed in the temperature range 77 - 300K. These compounds were paramagnetic in the measured temperature range, and the magnetic susceptibility obeyed the Curie-Weiss law. The lattice parameters obtained from X-ray diffraction powder data and the effective magnetic moments are listed in Table 1.

Table 1. Lattice parameters and μ_{eff} for $EuLn_2S_4$ samples obtained.

Samples obtained	Lattice constant a (Å)	μ_{eff} Observed	μ_{eff} Calculated
$EuLa_2S_4$	8.761	7.29	7.94
$EuCe_2S_4$	8.701	8.23	8.71
$EuPr_2S_4$	8.658	8.97	8.45
$EuNd_2S_4$	8.599	9.20	9.49
$EuSm_2S_4$	8.545	8.47	8.28
$EuGd_2S_4$	8.512	14.15	13.75

The values of μ_{cal} for $EuLn_2S_4$ were calculated as

$$\mu_{cal} = \sqrt{\mu^2_{Eu^{2+}} + 2\,\mu^2_{Ln^{3+}}}, \qquad (1)$$

where $\mu_{Eu^{2+}}$ and $\mu_{Ln^{3+}}$ expressed the effective magnetic moments of free Eu^{2+} and Ln^{3+} ions, respectively. Since calculated values of the magnetic moment for $EuLn_2S_4$ were in good agreement with the observed values, the Eu ion in these compounds was confirmed as divalent and the Ln ion as trivalent.

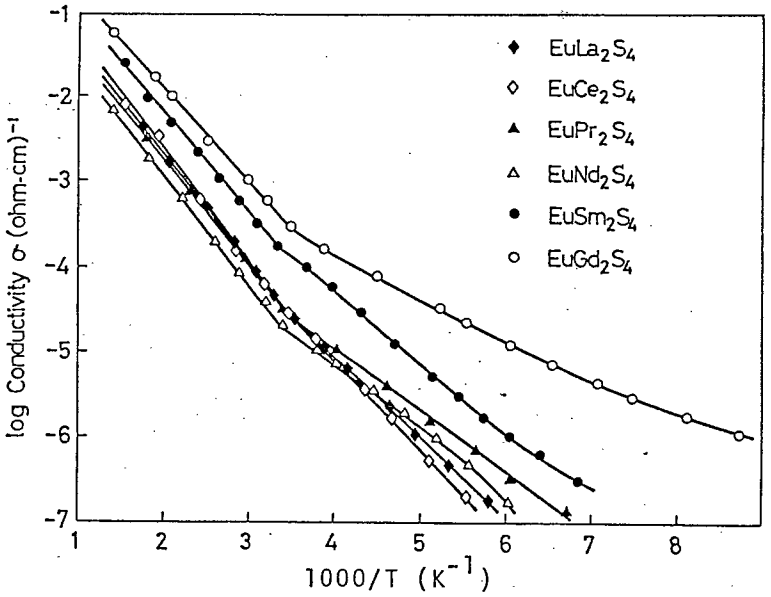

Fig. 3. Dependence of temperature on the electrical conductivity of $EuLn_2S_4$ in an atmosphere of He (at about 1 atm).

Electrical conductivity measurements were carried out in the temperature range 77 - 770K. The dependence of the electrical conductivities of $EuLn_2S_4$ on reciprocal of the temperature is shown in Fig. 3. All of the $EuLn_2S_4$ obtained behaved as semiconducting with Ω-cm values of the order of 10^4 - 10^5 at room temperature. From the qualitative estimation of thermoelectric power, the charge carrier for electrical conduction in all of these Th_3P_4-type $EuLn_2S_4$ was found to be positive. This finding represents a relatively unusual behavior among Th_3P_4-type compounds, most of which are metallic or n-type semiconducting materials. Although the precise band structure is unknown for these Th_3P_4-type compounds, it is presumed that the valence band is mainly associated with the 3p

states of sulfur and that the conduction band is made up of the 5d states of rare earths, analogous to the band model of europium monochalcogenides proposed by Wachter [15]. It is reasonable to assume that the 4f levels of rare earths are localized in a forbidden energy gap. Accordingly, positive holes may be created by ionizing the neutral electron accepter of a metal vacancy level above the top of the valence band.

As shown in Fig. 3, breaks in the log σ vs 1/T plots can be seen at approximately 300K for all compounds. Since no corresponding crystallographic or magnetic transitions were observed around this temperature, this electrical transport transition may represent the change from extrinsic to intrinsic semiconduction.

Other electrical properties are summarized in Table 2.

Table 2. Some of the electrical properties for $EuLn_2S_4$ samples obtained.

Samples obtained	Conductivity at 300°K, $\sigma \times 10^5$ $(\Omega\text{-cm})^{-1}$	Activation energy ε (eV)	
		At 300-700°K	At 130-300°K
$EuLa_2S_4$	3.05	0.25	0.12
$EuCe_2S_4$	3.39	0.26	0.16
$EuPr_2S_4$	3.16	0.24	0.10
$EuNd_2S_4$	2.70	0.25	0.15
$EuSm_2S_4$	15.5	0.23	0.16
$EuGd_2S_4$	36.3	0.22	0.10

The activation energy ε was calculated by the equation $\sigma=\sigma_0 \exp(-\varepsilon/kT)$. The values of the electrical conductivity at room temperature are almost constant on going from $EuLa_2S_4$

to $EuNd_2S_4$, but increase abruptly from $EuNd_2S_4$ to $EuGd_2S_4$. To understand the electrical properties of the Th_3P_4-type $EuLn_2S_4$ series, it is helpful to take into account the nature of chemical bonding in the $EuLn_2S_4$. The bond property can be appreciated by comparing the ionic and covalent radii of the corresponding elements in these compounds with the observed internuclear spacings. Miller et al. [16] proposed the concept of percent covalency as the covalent contribution to the bonding in the Th_3P_4 structure, using the equation,

$$\% \text{ covalency} = \frac{r_{s\ ion} - r_{s\ obs.}}{r_{s\ ion} - r_{s\ cov.}} \times 100, \quad (2)$$

where $r_{s\ ion}$, $r_{s\ cov.}$, and $r_{s\ obs.}$ are the ion, covalent, and observed radii of sulfur, respectively. Figure 4 shows the plots of the fraction of covalent bond character and the electrical conductivity at room temperature against atomic number. In $EuLn_2S_4$ with the Th_3P_4 structure, it appears that going from $EuLa_2S_4$ to $EuGd_2S_4$ makes the Ln-S bond less ionic. Ionic crystals are generally

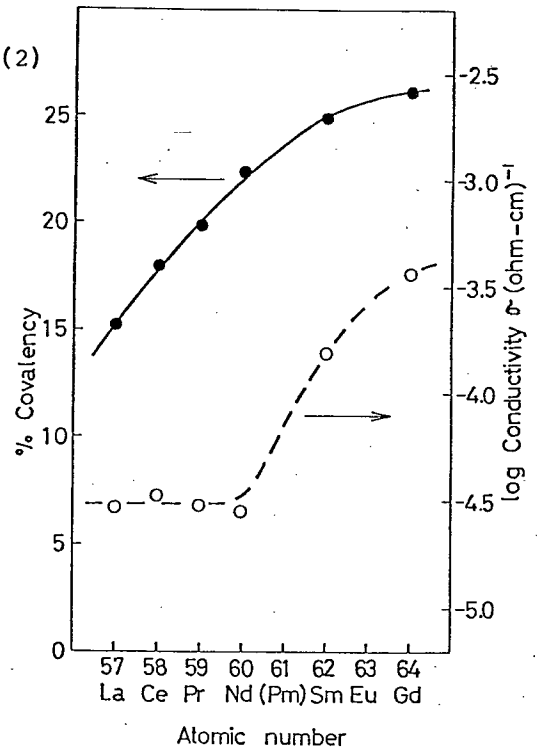

Fig. 4. Plots of the % covalency and the electrical conductivity at room temperature of $EuLn_2S_4$ against the atomic number of Ln components.

poor electrical conducting materials compared with covalent ones because of the former's small carrier mobility, resulting from their narrow bandwidths. This principle holds for the specimens obtained, except for $EuLa_2S_4$, $EuCe_2S_4$, and $EuPr_2S_4$. On the basis of the crystallographic considerations, for example, lattice energy, ionization energy, and strength of crystal field, it is understandable that metal vacancies are introduced more easily in ionic crystals than in covalent ones. Because in ionic crystals such as $EuLa_2S_4$, $EuCe_2S_4$, and $EuPr_2S_4$ the concentration of the positive hole increases with increase of these metal vacancies, these compounds seem to have higher electrical conductivities than are expected from their percent covalency.

The behavior of the conductivity in sulfur vapor for $EuGd_2S_4$ is shown in Figs. 5 and 6. The time dependence of the electrical conductivity in various sulfur pressures is illustrated in Fig. 5. The higher the sulfur pressure was, the more time was required to reach the equilibrium of the conductivity. This fact suggests that a

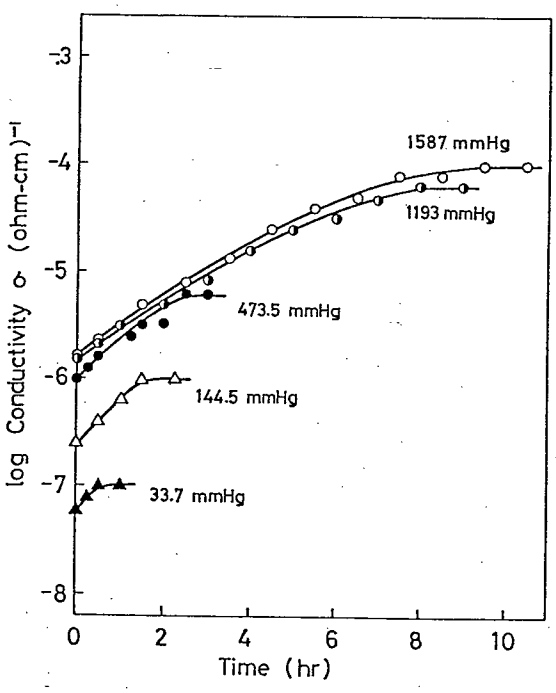

Fig. 5. Time dependence on the electrical conductivity of $EuGd_2S_4$ in various sulfur pressures at 500°C.

thin layer exists in grain boundaries of the sintered sample and that the sulfur passage through such a layer to the bulk is the rate-determining stage for the diffusion of sulfur into $EuGd_2S_4$. Figure 6 shows the plots of logarithmic conductivity σ vs logarithmic sulfur pressure P_{S_2}. The conductivity values increased as the sulfur increased, and the slope of log σ vs log P_{S_2} was 1/5.9 at all temperatures. This positive variation is usually observed in p-type metal oxide or sulfide semiconductors, such as NiO or PbS. For the increase of electrical conductivity under high sulfur pressure, the following two processes may be taken into account by equation (3) or (4),

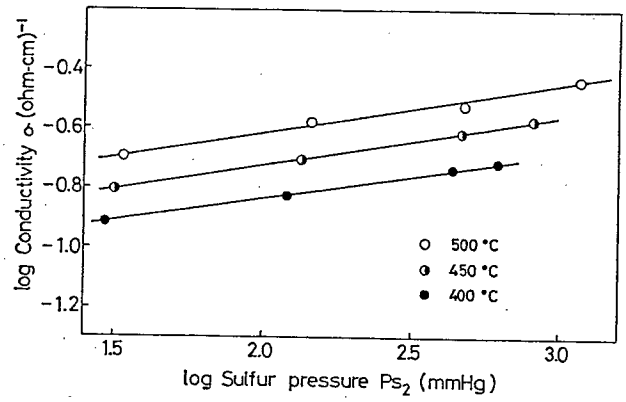

Fig. 6. Dependence of sulfur pressure on the electrical conductivity of $EuGd_2S_4$ at various temperatures.

$$1/2\ S_2 \rightleftharpoons S_S + V_{Eu}' + h^{\cdot}, \quad (3)$$

$$1/2\ S_2 \rightleftharpoons S_S + V_{Eu}'' + 2\ h^{\cdot}, \quad (4)$$

where S_S represents S atom on a normal lattice site, V_{Eu}' a singly and V_{Eu}'' a doubly ionized Eu vacancy, and $h^{\cdot}$ a positive hole. The generation of Eu vacancy is accelerated by the transition of Eu^{2+} to Eu^{3+}. The following relationships can be obtained by adapting the mass action law to equations (3) and (4):

$$\sigma \propto [h^{\cdot}] \propto P_{S_2}^{1/4}, \tag{5}$$

$$\sigma \propto [h^{\cdot}] \propto P_{S_2}^{1/6}. \tag{6}$$

Equation (6) is in agreement with the results in Fig. 6, where the values of the slopes in log σ vs log P_{S_2} plots were 1/5.9. The dependence of the electrical conductivity on the inverse of the sixth power of logarithmic sulfur pressure, illustrated in Fig. 6, clearly indicates that the reaction (4) takes place at constant temperature over the range 400 to 500°C and thermodynamic equilibrium with the sulfur vapor.

b) Nonstoichiometric $EuGd_2S_4$

Table 3 shows the atomic ratio of $EuGd_2S_4$ heated at various temperatures in vacuo. The composition of the nontreated sample was slightly different from that of the stoichiometric sample. This difference is presumably due to an analytical error, but the nontreated $EuGd_2S_4$ may be approximately taken as in stoichiometry. Heat treatment under high temperatures and a high vacuum decreased the concentration of both Eu and S components in $EuGd_2S_4$. These

Table 3. Atomic ratio of the samples obtained by heating $EuGd_2S_4$ at various temperatures.

Heating temp. (°C)	Atomic ratio Eu : Gd : S		
Nontreated	1.02	2	3.99
1500	1.01	2	3.98
1600	0.98	2	3.88
1700	0.88	2	3.81
1800	0.83	2	3.80

components seem to subline in the form of EuS and sulfur molecules. The final composition is regarded as Gd_3S_4. However, this compound actually decomposed upon heating at temperatures higher than 1900°C.

Data on X-ray powder diffraction and magnetic measurements are given in Table 4. The X-ray powder diffraction patterns

Table 4. Lattice constants and magnetic data of the nonstoichiometric $EuGd_2S_4$ samples.

Heating temp. (°C)	Lattice const. (Å)	μ_{cal} (μ_B)	μ_{eff} (μ_B)	θ_p (°K)
Nontreated	8.512	13.82	14.15	1.0
1500	8.518	13.82	13.54	5.6
1600	8.502	13.91	13.39	14.5
1700	8.499	13.80	13.31	27.5
1800	8.465	13.71	13.38	34.5

of the heated samples were all indexed on the cubic Th_3P_4 structure. Since the diffuse X-ray diffraction patterns were obtained for the samples heated at higher temperatures, the samples seem to become poorer crystalline.

The magnetic susceptibility for all the samples was measured in the range 77 - 300K. The susceptibilities obeyed the Curie-Weiss law in this range. Analysis of the linear portion of the $1/\chi_M$ vs T curve yields values of μ_{eff}, which are close to the theoretical ones. On the other hand, it is very interesting that the heated materials possess a positive paramagnetic Curie temperature θ_p. On the basis of this result, nonstoichiometric $EuGd_2S_4$ samples are expected

to become ferromagnetic materials at low temperatures, though stoichiometric $EuGd_2S_4$ is antiferromagnetic as reported by Lugscheider et al. [14].

Electrical conductivity measurements were performed in the range 77 - 770K. The temperature dependences of the conductivity are shown in Fig. 7. The conductivity of the heated samples was very high compared with that of the non-treated one. The samples heated at 1500°C and 1600°C have semiconducting behavior, while those heated at 1700°C and 1800°C are metallic. The increase in conductivity resulting from the heat treatment does not seem to correspond to increase of mobility but to increase of the number of conduction electrons, which are supplied to a partially filled 5d band due to the removal

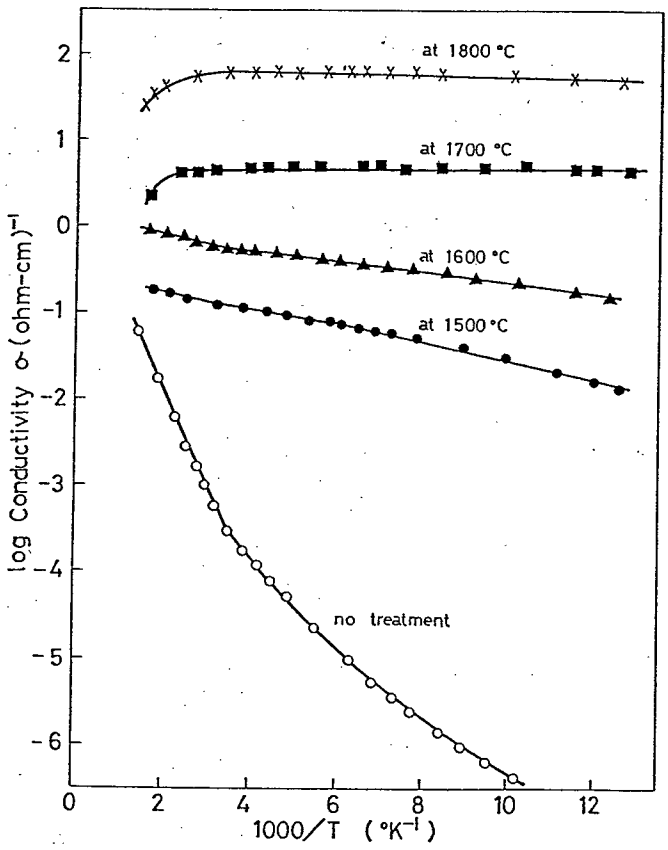

Fig. 7. Temperature dependence on the electrical conductivity of $EuGd_2S_4$ heated at various temperatures in vacuo.

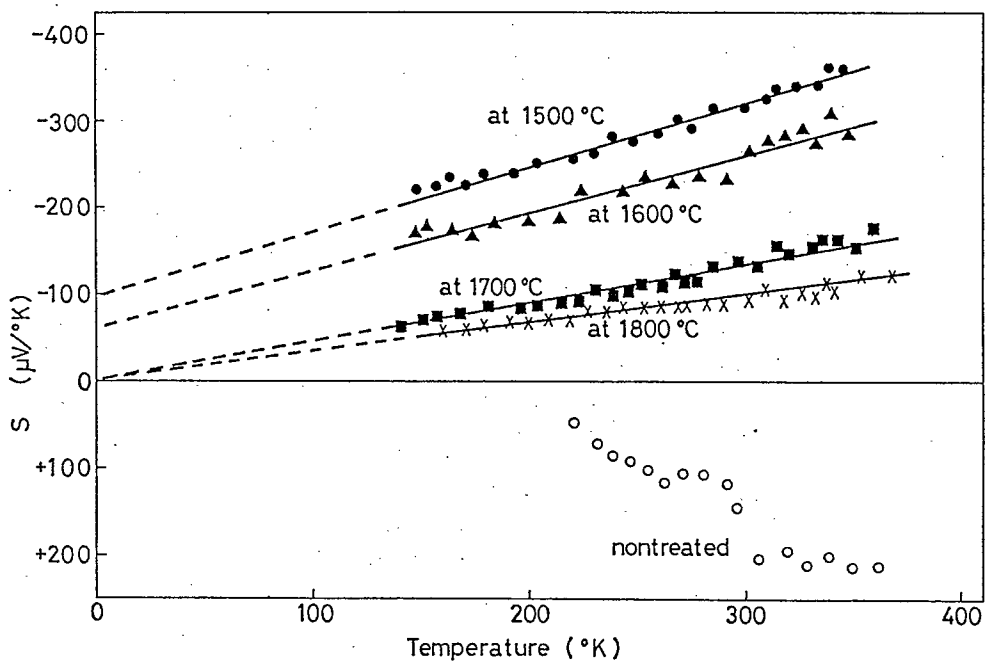

Fig. 8. Temperature dependence of the thermoelectric power of $EuGd_2S_4$ heated at various temperatures.

of sulfur.

Figure 8 shows the temperature dependence of the thermoelectric power. The sign of the thermoelectric power S in all heated specimens is negative over the whole range of temperatures, indicating electron-type conduction, while the sign of the nontreated materials is positive. Linearity of the thermoelectric power S vs temperature T was obtained for all heated specimens. The temperature dependences of S can be classified into two categories: (I) the metallic materials, whose intercept of the S vs T plot at T=0 is about zero; (II) the semiconductors, whose intercept at T=0 corresponds to a finite value of S.

In the nearly free electron approximation the thermoelectric power S is commonly represented by

$$S = -\frac{\pi^2 k^2 T}{3e}\left(\frac{\partial \ln\sigma}{\partial E}\right)_{E=E_f}, \tag{7}$$

where E_f is the energy of the Fermi level at temperature T, k is the Boltzmann constant, and σ is the conductivity at energy E. Assuming that the carriers are chiefly scattered by lattice vibrations in the metallic materials, in order to simplify the problem, equation (7) reduces to the form

$$S = -\frac{\pi^2 k^2}{3e}\frac{T}{E_f}. \tag{8}$$

By means of equation (8) we can make a rough estimate of the Fermi energy E_f. The values of E_f calculated from the experimental values of the thermoelectric power are given in Table 5 for the samples heated at 1700°C and 1800°C.

In cerium sulfide $Ce_{3-x}S_4$, each conduction electron is to be thought of as moving in the d band under the influence of the

Table 5. Electrical transport properties of nonstoichiometric $EuGd_2S_4$ samples.

Heating temp. (°C)	Conductivity σ at 300°K $(\Omega\text{-cm})^{-1}$	Type of conduction	Activation energy (eV)	Fermi energy (eV)
Nontreated	3.63×10^{-6}	p-type semi	0.10-0.22	-
1500	1.22×10^{-1}	n-type semi	0.02	-
1600	5.52×10^{-1}	n-type semi	0.013-0.027	-
1700	4.51	Metallic	-	0.037
1800	5.94×10	Metallic	-	0.101

fluctuating random field due to the negative charges on the cation vacancies. This situation can be applied to the nonstoichiometric $EuGd_2S_4$ dealt with in this chapter, since a number of cation vacancies are produced by the sublimation of Eu atom. The conduction in such a case is via electron hopping from one localized state to another, and its mobility μ contains an activation energy W. As shown by Cutler and Mott [12], the conductivity σ in this type of conduction is represented by

$$\sigma = \sigma(E_f) = e\mu(E_f)N(E_f)kT, \tag{9}$$

where
$$\mu(E) = \mu_0(E)\exp(-W/kT), \tag{10}$$

and
$$\mu_0 = C/kT. \tag{11}$$

N(E) is the electron density at energy E, and C is a constant. When equation (9) is substituted in equation (7), one obtains

$$S = -\frac{\pi^2 k}{3e}\left[kT\frac{d\ln(\mu_0 N)}{dE} - \frac{dW}{dE}\right]. \tag{12}$$

Thus, S should be a linear function of T for which the slope and intercept yield values of $d\ln(\mu_0 N)/dE$ and dW/dE for $E=E_f$. This is found to be true for the case of the semiconductors, that is, the samples heated at 1500°C and 1600°C. The activation energy for the hopping conduction is given in Table 5.

The electrical behaviors of nonstoichiometric $EuGd_2S_4$ samples can be explained with the model proposed by Cutler

and Mott, as follows. One expects the density of states curve to be broader than it would be without the random field, and a tail in which the states are localized as shown in Fig. 9.

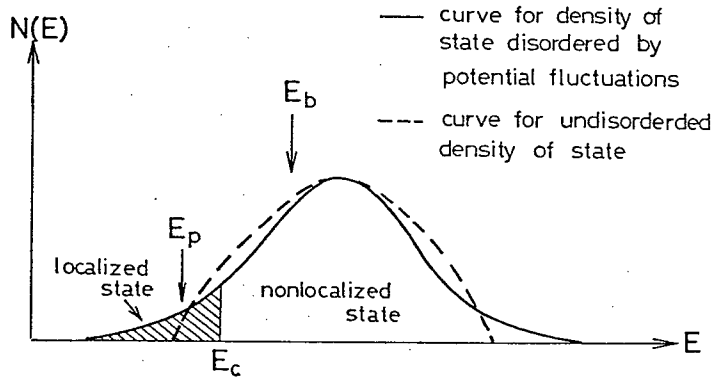

Fig. 9. Sketch of curves for density of states. E_p is the Fermi energy for low concentrations of electrons for which conduction is by hopping, E_b for high concentrations. E_c is a critical energy.

One denotes by E_c the energy separating state, "mobility edge", which is localized from that which is not. Then, if the Fermi energy E_f lies below E_c, the conductivity tends to zero with decreasing temperature; if E_f lies above E_c, the conductivity tends to a finite value. For the case of $E < E_c$ ($E_f = E_p$ which is the fermi energy for low concentrations of electrons), the conduction is by electron hopping between localized states, and the mobility contains an activation energy $W(E)$, which is expected to tend to zero as $E \to E_c$. This case may be true for the semiconducting materials. For the case of $E > E_c$ ($E_f = E_b$ which is the Fermi energy for high concentrations of electrons), the conduction is the ordinary band conduction, which may be true for the metallic materials.

1-4 Summary

Electrical transport properties of stoichiometric and nonstoichiometric rare earth sulfides, $EuLn_2S_4$, were studied. The results obtained in this chapter are summarized as follows.

1. Th_3P_4-type $EuLn_2S_4$ (Ln = La - Gd) compounds are all p-type semiconductors, and their conductivities at room temperature have almost the same value for the specimens from $EuLa_2S_4$ to $EuNd_2S_4$ but increase on going from $EuNd_2S_4$ to $EuGd_2S_4$. These behaviors can be explained on the basis of the concept of percent covalency as the covalent contribution to the bonding in the Th_3P_4 structure.

2. The conductivity of $EuGd_2S_4$ is sensitive to sulfur vapor pressure, obeying the relationship $\sigma \propto P_{S_2}^{1/6}$. From this result, the following equilibrium reaction is found to take place at the constant temperature over the range 400 - 500°C, and the thermodynamic equilibrium with sulfur vapor.

$$1/2\ S_2 \rightleftharpoons S_S + V_{Eu}'' + 2\ h^{\cdot}$$

3. The heat treatment of stoichiometric $EuGd_2S_4$ under high temperatures and a high vacuum decreases the concentrations of both Eu and S components. The samples heated were classified into two groups on the basis of their electrical transport behaviors. One group comprises semiconducting materials heated at 1500°C and 1600°C, for which the transport mechanism is found to be via electron hopping with activation energies ranging from 0.013 eV to 0.027 eV. Another group comprises

metallic materials heated at 1700°C and 1800°C. Their electrical transport is carried out through an ordinary band conduction.

Chapter 2

Electrical and Magnetic Properties of Mixed Valence Rare Earth Sulfides, $(Sm_{1-x}Gd_x)_3S_4$

2-1 Introduction

There has been a great interest in the mixed valence compounds, such as rare earth systems involving Ce, Sm, Eu, Tm, and Yb. Especially in the materials with divalent samarium ions like SmS, the electrical occupation of the 4f shell changes readily with increasing temperature or external pressure, accompaning the discontinuous variations of some physical properties [17-20].

Another samarium sulfide, Sm_3S_4, which also has divalent samarium ions, is classified as an heterogeneous mixed valence compound, whereas SmS is a homogeneous one. In Sm_3S_4 which crystallizes in the cubic Th_3P_4-type structure, divalent and trivalent Sm ions occupy equivalent lattice sites [21,22]. From Mössbauer measurements for Sm_3S_4, Eibschütz et al. [23] have found that the valence fluctuations in samarium ions are thermally activated, and therefore, the valence fluctuation rate may be varied with temperature. These valence fluctuations can be described by the "hopping model" [24] with thermally activated electron hopping between cations of different valences. The hopping conduction in Sm_3S_4 was confirmed by electrical conductivity [25,26], Hall effect [26], and thermoelectric power [26] measurements. On the other

hand, gadolinium sulfide, Gd_3S_4, which also crystallizes in the Th_3P_4 structure, possesses one conduction electron in one unit formula, since Gd ions involved are trivalent. The substitution of the Sm ion in Sm_3S_4 with a smaller Gd^{3+} ion is expected to have some influences on the valence state of Sm ions, because the substitution may cause the internal compression in the crystal as observed in $Sm_{1-x}Gd_xS$ [7,17,27].

From this point of view, the electrical and magnetic properties of $(Sm_{1-x}Gd_x)_3S_4$ solid solutions are investigated and the valence transition of samarium ions in these mateials are discussed.

2-2 Experimental

Preparation of samples

Samples were prepared by the following two-step procedures. First, samarium or gadolinium monosulfide was obtained by a direct reaction of sulfur powder with Sm or Gd metal in an evacuated, sealed quartz tube at 600°C for 24 hr and then at 1000°C for 5 hr. Sesquisulfides, Sm_2S_3 and Gd_2S_3, were obtained by the method described in chapter 1. Second, polycrystalline $(Sm_{1-x}Gd_x)_3S_4$ samples were prepared by the following solid state reaction in an induction furnace at 1600°C for 3 hr in vacuum ($\sim 10^{-4}$ mmHg).

$$(1-x)(SmS + Sm_2S_3) + x(GdS + Gd_2S_3) \longrightarrow (Sm_{1-x}Gd_x)_3S_4 \qquad (13)$$

Analyses

The atomic ratio (Sm : Gd) in the samples was determined by a Rigaku Denki X-ray Fluorescent spectrometer equipped with a Si(Li) detector. The quantity of sulfur was determined by the same method described in chapter 1. The analytical values obtained agreed with the nominal values within an experimental error.

Measurements of some physical properties

Electrical conductivity measurements were carried out in an atmosphere of He (at about 1 atm) over the temperature range 4.2 - 300K. The data were obtained by a four-probe method, using a direct current.

Magnetic susceptibility data were obtained with a Shimadzu magnetic balance BM-11 which was modified for the measurements in the temperature range 4.2 - 300K.

The structure of resulting materials was characterized by X-ray powder data from a Rigaku Denki "Rota-flex" diffractometer with a scintillation detector and a CuK_{α} radiation. The lattice parameters were refined by the least squares method for unambigously indexed reflections calibrated with high purity Si (99.999 %).

Reflection spectra of powder samples were obtained with a Shimadzu double beam spectrophotometer UV-180 in the wavelength region from 300 nm to 700 nm. The reflectance of samples was determined by regarding the reflectance of MgO powder as 100 %.

X-ray photoemission spectra were obtained with a Shimadzu ESCA 650B electron spectrometer, using a MgK_{α} radiation. All experiments were carried out under a vacuum of 10^{-7} mmHg. The

binding energy in X-ray photoemission spectra (XPS) obtained was calibrated by the position of the contaminating cabon 1s peak.

2-3 Results and discussion

a) Electrical and optical properties

The X-ray powder diffraction patterns for the solid solutions obtained were all indexed on the basis of the Th_3P_4 structure. Figure 10 shows the lattice parameter variations with the composition for the $(Sm_{1-x}Gd_x)_3S_4$ system at room temperature. The Vegard's law evidently does not hold for this system. This departure from the Vegard's law seems to suggest some changes in the valence of the containing ions, which is perhaps the samarium ion rather than the gadolinium ion. The solid line in Fig. 11 shows the electrical conductivity at 300K. The conductivity

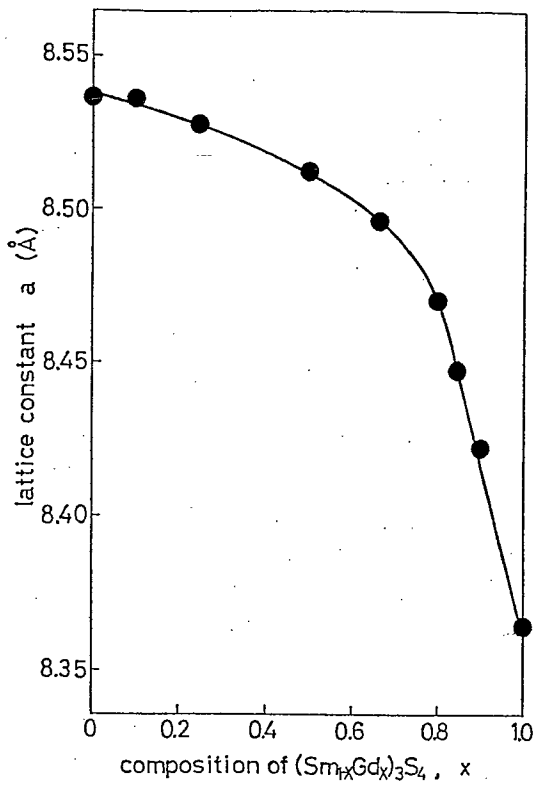

Fig. 10. Lattice parameter of $(Sm_{1-x}Gd_x)_3S_4$ as a function of composition.

of the materials gradually decreases up to x=0.80 with increasing Gd concentration, in spite of mixing metallic Gd_3S_4 with semiconducting Sm_3S_4. A drastic change from the semiconducting to metallic conduction, however, was observed at the composition range between x=0.80 and x=0.85. As is shown in Figs. 10 and 11, the composition at which the lattice parameter vs

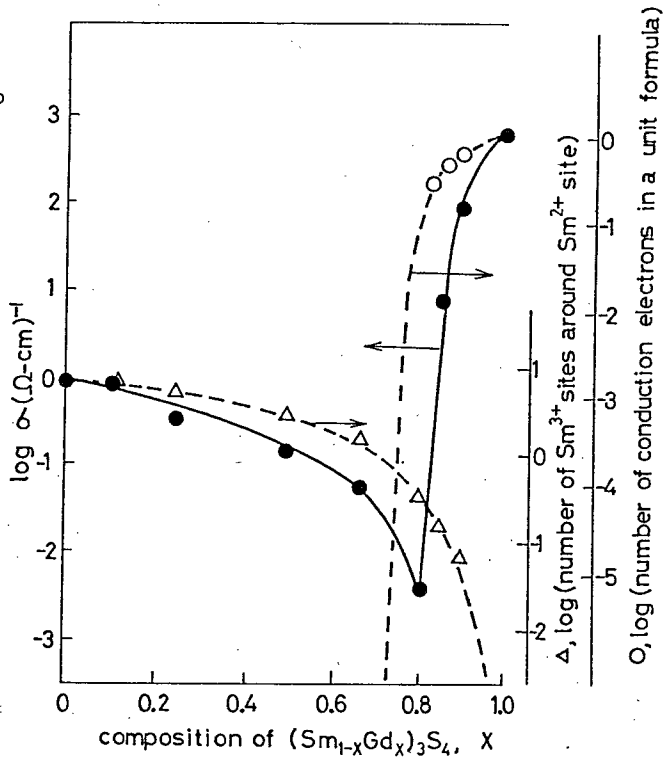

Fig. 11. Electrical conductivity at room temperature of $(Sm_{1-x}Gd_x)_3S_4$ —●—, number of Sm^{3+} sites around Sm^{2+} site -△-, and number of conduction electrons in an unit formula -○-, as a function of composition.

composition curve breaks approximately coincides with the composition at which the drastic change in the conductivity was observed. However, this change in $(Sm_{1-x}Gd_x)_3S_4$ seems to be essentially different from the transition in $Sm_{1-x}Gd_xS$ [5,15], because no discontinuous changes in the crystal volume were found to be in this system.

The electrical conductivity of Sm_3S_4 has displayed a semiconducting behavior, increasing with the rise of temperature as $\sigma \propto \exp(-\varepsilon/kT)$, where ε is equal to 0.16 eV. This value

is in good agreement with the published data [28]. The temperature dependences of the electrical conductivity for the semiconducting materials ($0 \leqslant x \leqslant 0.80$) are shown in Fig. 12. A gradual departure from the linearity can be seen in the curve of log σ vs reciprocal temperature for the $(Sm_{0.2}Gd_{0.8})_3S_4$ sample below about 240K. Since this sample is a poor conductor, the departure is probably due to the impurities existed in grain boundaries.

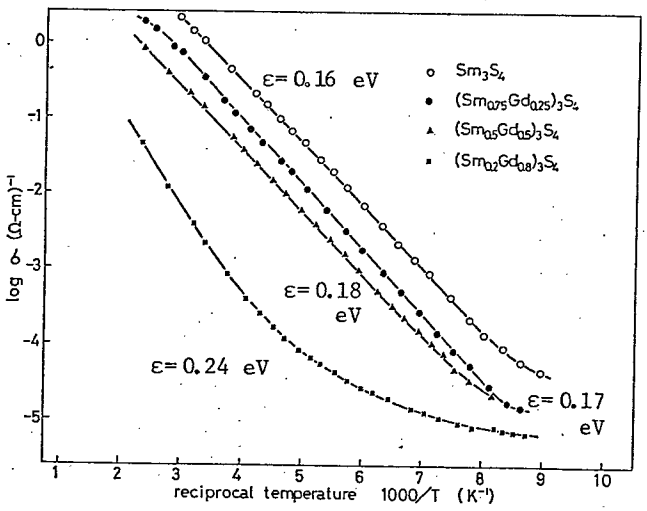

Fig. 12. Temperature dependence of electrical conductivity for semiconducting $(Sm_{1-x}Gd_x)_3S_4$.

In order to understand the electrical behavior of $(Sm_{1-x}Gd_x)_3S_4$, the valence change of Sm ions was investigated. The valence of the Sm ions in mixed valence compounds, e.g., $Sm_{1-x}Gd_xS$ and SmB_6, can be deduced from the lattice constants, magnetic susceptibilities, or Mössbauer effect [29-32]. Here, the fraction, y, of Sm^{3+} ion to the total Sm ions in $(Sm_{1-x}Gd_x)_3S_4$ was estimated from the lattice constant for each solid solution, using the following equation

$$(1-y)\, R_{Sm^{2+}} + y\, R_{Sm^{3+}} = R_{obs.}, \qquad (14)$$

where $R_{Sm^{2+}}$ and $R_{Sm^{3+}}$ express the radii of the Sm^{2+} and Sm^{3+}

ions, equal to 1.41 Å and 1.219 Å respectively, and $R_{obs.}$ the average Sm ion radius which is obtained from the observed lattice constant, using the ionic radius for Gd^{3+} ion (1.193 Å) and for S^{2-} ion (1.70 Å) proposed by Shannon [33]. The results obtained are given in Table 6. The obtained value

Table 6. Lattice constants and some related data for $(Sm_{1-x}Gd_x)_3S_4$.

Composition	Lattice constant (Å)	Fraction of Sm^{3+} ions in Sm ions (%)	Number of Sm^{3+} sites around Sm^{2+} sites	Number of electrons in an unit formula
Sm_3S_4	8.543	82	8	0
$(Sm_{0.9}Gd_{0.1})_3S_4$	8.532	79	6.9	0
$(Sm_{0.75}Gd_{0.25})_3S_4$	8.527	74	5.4	0
$(Sm_{0.5}Gd_{0.5})_3S_4$	8.512	61	3.0	0
$(Sm_{0.333}Gd_{0.667})_3S_4$	8.494	45	1.5	0
$(Sm_{0.2}Gd_{0.8})_3S_4$	8.473	18	0.35	0.31
$(Sm_{0.15}Gd_{0.85})_3S_4$	8.448	10	0.15	0.48
$(Sm_{0.1}Gd_{0.9})_3S_4$	8.427	7	0.07	0.64
Gd_3S_4	8.370	-	-	1

of the Sm^{3+} fraction for pure Sm_3S_4 sample was 82 %. If one takes into account the charge balance as $Sm^{2+}Sm_2^{3+}S_4^{2-}$, the fraction of Sm^{3+} ion should be 67 %. This discrepancy can be regarded as follows. In the semiconducting black phase of $Sm_{1-x}Gd_xS$ system, the valence of the Sm ion deduced from the lattice constants is known to be +2.2, indicating that the fraction of Sm^{3+} ion is not 0 % but 20 % [27,28]. Thus, the electrons which have left the 4f shell of Sm^{2+} ion in Sm_3S_4 do not seem to enter the d conduction band as free charge

carriers but remain mostly localized just below Fermi level in the same manner as the $Sm_{1-x}Gd_xS$ system. Apparently from Fig. 13, the valence transition from trivalent to divalent Sm ions with increasing Gd content was found to exist in this system. This means that the Sm^{3+} ion is reduced into the Sm^{2+} ion by the conduction electrons introduced from metallic Gd_3S_4.

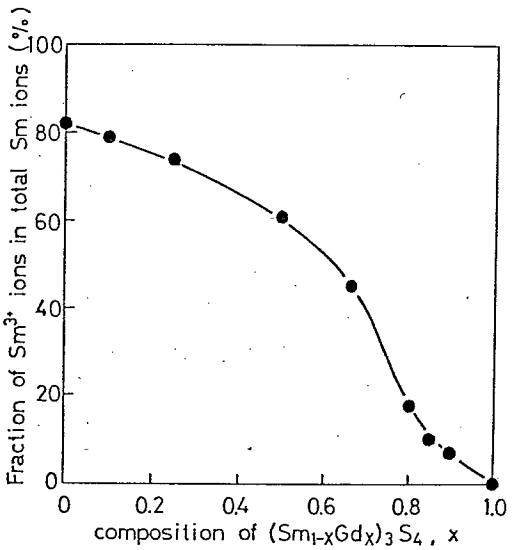

Fig. 13. Fraction of Sm^{3+} ion to the total Sm ions in $(Sm_{1-x}Gd_x)_3S_4$.

As is suggested by Smirnov et al. [26], the electrical conduction process in Sm_3S_4 is a thermally activated hopping of the charge carriers between the Sm^{2+} and Sm^{3+} sites. In this study, the electrical behaviors of $(Sm_{1-x}Gd_x)_3S_4$ at room temperature are discussed from the viewpoint of the hopping conduction between Sm sites. Assuming that the hopping of electrons is the sole workable mechanism for the electrical transport of $(Sm_{1-x}Gd_x)_3S_4$, the number of nearest neighboring Sm^{3+} sites around the Sm^{2+} site would be proportional to the electrical conductivity. In the Th_3P_4 structure a cation site is surrounded by eight nearest neighboring cation sites as shown in Fig. 1. In order to simplify the positional situation of Sm sites, it can be assumed for Sm_3S_4 that a divalent Sm site is surrounded by eight trivalent Sm sites in

the same manner as $EuGd_2S_4$ [14]. For the solid solutions, the number of Sm^{3+} sites around a Sm site was roughly estimated by taking into account the substitution of the Sm^{3+} ion with the Gd^{3+} ion and the reduction of remaining Sm^{3+} ion by the electrons from metallic Gd_3S_4. On the other hand, the number of conduction electrons for the metallic solid solutions with high Gd contents was obtained from the difference between the number of electrons from Gd_3S_4 and the number of Sm^{3+} sites of Sm_3S_4 in the starting materials. This estimation is based on the fact that the Sm^{3+} ions in the starting material were reduced by Gd_3S_4 during the formation of the solid solution. At a constant temperature, these values for the number of Sm^{3+} sites and the conduction electrons should be parallel to the magnitudes of the hopping and the metallic band conductions respectively. Logarithm of these values is plotted as a function of the composition in Fig. 11 (dashed lines). Though the magnitudes of the hopping and the metallic conductions for $(Sm_{1-x}Gd_x)_3S_4$ are roughly estimated from simple assumptions, the calculated results are substantially consistent with experimental results. This fact suggests that above assumptions of the hopping and the metallic conductions for each solid solution is reasonable.

The existence of two Sm valence states in $(Sm_{1-x}Gd_x)_3S_4$ was directly verified by the X-ray photoemission measurements. Figure 14 shows X-ray photoemission spectra (XPS) for the sintered Sm_3S_4, $(Sm_{0.75}Gd_{0.25})_3S_4$, and $(Sm_{0.5}Gd_{0.5})_3S_4$ samples after being etched by the argon beam for 5 minute at room temperature. Although the fine structure of the 4f multiplets

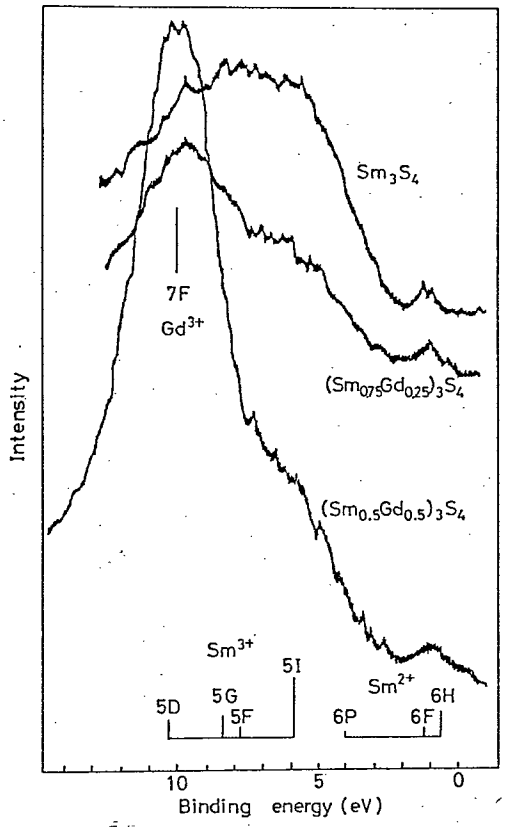

Fig. 14. XPS spectra for $(Sm_{1-x}Gd_x)_3S_4$ after being etched by argon beam for 5 minute at room temperature.

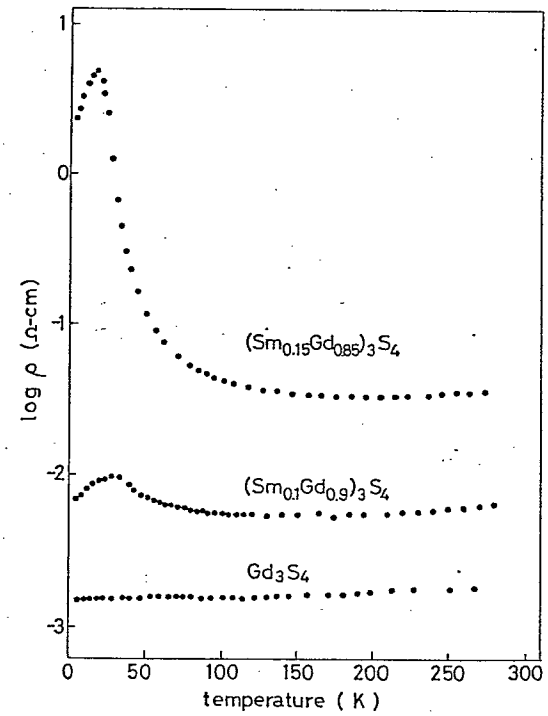

Fig. 15. Temperature dependence of electrical resistivity of metallic $(Sm_{1-x}Gd_x)_3S_4$.

for each Sm^{2+} and Sm^{3+} ion was not clearly resolved, the characteristics spectra of both Sm^{2+} and Sm^{3+} ions can be seen. Two peaks which correspond to the 5I state of $4f^6$ (Sm^{2+}) and to the 6H state of $4f^5$ (Sm^{3+}) [34] are respectively observed at about 1 eV and 6 eV. The failure to resolve the 4f multiplets for Sm^{2+} and Sm^{3+} ions may be due to the hopping of 4f electrons.

The measurements of the temperature dependence of the electrical resistivity for the metallic samples were carried

out at the range 4.2 - 300K. The results obtained are shown in Fig. 15. Maxima of the resistivity were observed in the curves of resistivity vs temperature. For the $(Sm_{0.15}Gd_{0.85})_3S_4$ sample the resistivity value at 20K was larger than at 300K by a factor of about 10^2. This large maximum in the resistivity seems to be similar to that observed in the ferromagnetic $Eu_{1-x}Gd_xS$ system [35], since the transition to the ferromagnet was observed in all metallic samples at low temperatures, as is to show in the next section. This Curie temperature was approximately in agreement with the temperature at which the maximum in resistivity emerged. The magnitude of the maximum in resistivity increases as the Curie temperature decreases. Kasuya et al. [36] have theoretically studied the properties of a magnetic polaron in a magnetic semiconductor and suggested that the polaron was formed most easily for a small bandwidth and a small positive paramagnetic Curie temperature (nearly equal to the Curie temperature). From this point of view, it seems that the resistivity maxima observed in metallic samples are due to the formation of magnetic polarons which result from the magnetic interaction between the spins of conduction electrons and the spins of the 4f electrons of Gd^{3+} ions. The details with respect to these phenomena are to be discussed in the next chapter.

Figure 16 shows the reflection spectra of $(Sm_{1-x}Gd_x)_3S_4$ solid solutions in the 300 - 700 nm range. Since the measurements were carried out in the form of powders, the spectra obtained were very broad. Clear reflection maxima

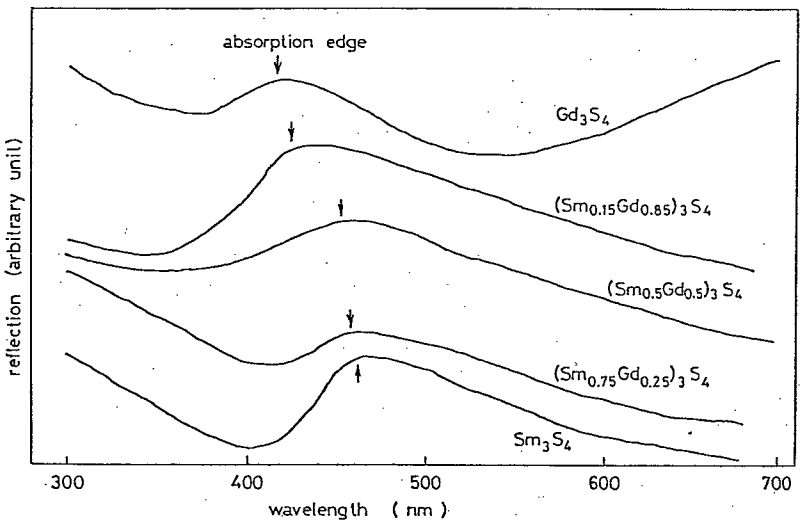

Fig. 16. Reflection spectra of $(Sm_{1-x}Gd_x)_3S_4$.

are, however, observed at 400 - 470 nm and their positions are strongly dependent on the composition of the solid solutions. It seems that these reflection maxima are due to a certain fundamental absorption edge. The plot of the absorption edge energy vs the composition of solid solutions gives a linear relationship as shown in Fig. 17. From the analogy to the published energy level schema of samarium and gadolinium mono-

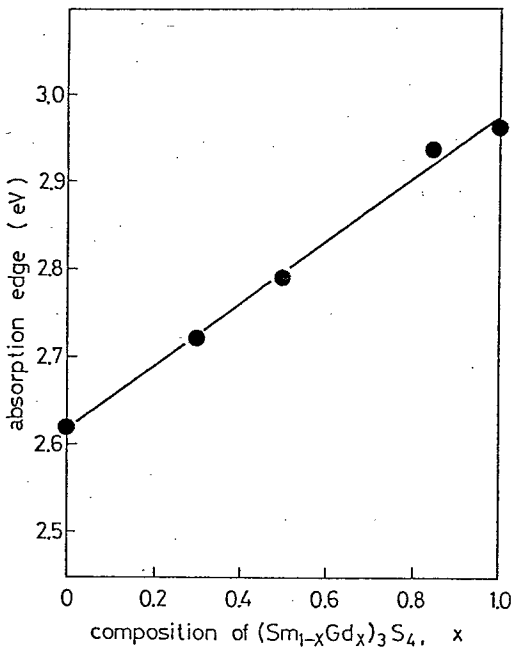

Fig. 17. Plot of absorption edge energy vs composition of $(Sm_{1-x}Gd_x)_3S_4$.

chalcogenides [37,38], it is considered that in $(Sm_{1-x}Gd_x)_3S_4$ the Sm^{3+}-$4f^5$ and Gd^{3+}-$4f^7$ states lie below the 2p valence band of the sulfur ions and that the Sm^{2+}-$4f^6$ state lie just below the 5d conduction band of the rare earth ions. At this point of view, the electronic transitions observed in the reflection spectra (Fig. 16) would not be associated with these 4f states of the rare earth ions but with the band gaps between the valence and the conduction bands. For Sm_3S_4 sample, the band gap determined from the reflection measurement was 2.63 eV. The band gap for La_2S_3 and Dy_2S_3 single crystals with the Th_3P_4 structure are reported to be 2.8 ± 0.1 eV and 2.85 ± 0.1 eV, respectively, determined from optical properties [39]. Thus, the value of the band gap obtained for Sm_3S_4 is regarded as a reasonable one.

These band gaps are not directly correlated with the activation energies in the electrical conduction of the solid solutions as shown in Fig. 12. As is mentioned before, the electrical conduction process in Sm_3S_4 is a hopping of electrons between Sm^{2+} and Sm^{3+} sites. The activation energy for the hopping conduction is, therefore, greatly dependent on the Sm^{2+}-$4f^6$ state and contains a thermally activated drift mobility. No reflection peaks associated with the Sm^{2+}-$4f^6$ state were observed in our measurements. The energy of the electronic transition from the $4f^6$ state to the conduction band is thought to be less than 1 eV, as shown in the XPS spectra (Fig. 14). The origin of the localization of electrons attributed to the hopping conduction is not clear. It may be due to the strong electron-phonon interactions,

leading to the formation of small polaron states.

b) Magnetic properties

A divalent Sm ion has the $4f^6$ configuration, for which the Russell-Saunders ground state is non-magnetic $^7F_0$. This configuration leads to van Vleck's paramagnetism similar to Eu^{3+} compounds. Figure 18 shows the susceptibility of the Sm_3S_4 obtained in this experiment at the temperature range between 4.2K and 300K. The constant susceptibility was found to exist between 50K and 100K, and seems to be due to a magnetic $^7F_1$ first excited state of the divalent Sm ion. The susceptibility of van Vleck's paramagnetism is expressed in [40]

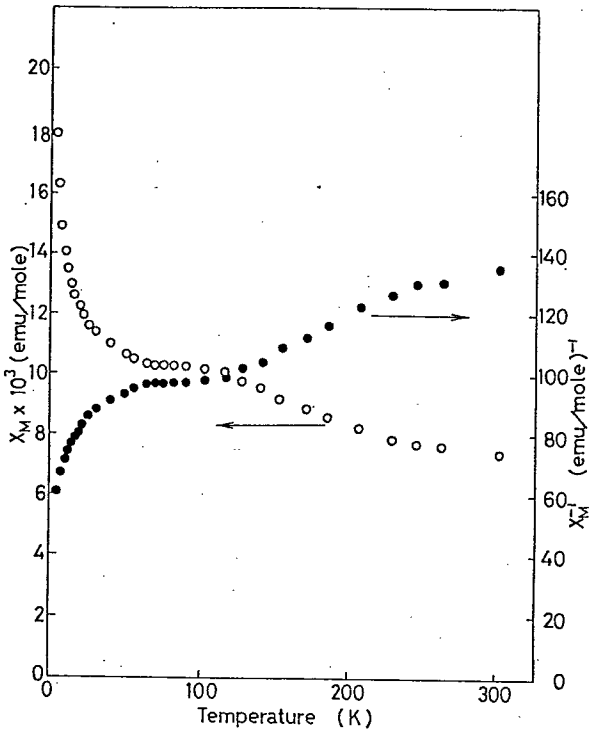

Fig. 18. Temperature dependence of magnetic susceptibility for Sm_3S_4.

$$\chi\ (T = 0) = \frac{8N\mu_B^2}{E_{J=1} - E_{J=0}}, \qquad (15)$$

where the denominator is the energy difference between the first excited state and the ground state of the spin-orbital coupling. Thus, this susceptibility is independent of temperature. An upturn in the susceptibility vs temperature curve was observed below 50K, analogous to that observed in SmS [41], but its strength is larger than that of SmS. This behavior is probably due to the high concentration of the trivalent Sm ($4f^5$) ion which has the magnetic ground state $^6H_{5/2}$. Escorne et al. [42] have pointed out that the magnetic susceptibility of the Sm_3S_4 material with an ideal $Sm^{2+}Sm_2^{3+}S_4^{2-}$ composition is composed of $\chi_{Sm^{2+}} + 2\chi_{Sm^{3+}}$ at low remperatures. One can estimate the fraction of Sm^{3+} ions in the Sm_3S_4 sample obtained in this study, using the equation

$$(1-y)\ \chi_{SmS}^{(sc)} + y\ \chi_{SmS}^{(m)} = 1/3\ \chi_{obs.}\ , \qquad (16)$$

where $\chi_{SmS}^{(sc)}$ is the susceptibility of the semiconducting phase SmS and corresponds to that of Sm^{2+}, $\chi_{SmS}^{(m)}$ the susceptibility of the metallic phase SmS, associated with Sm^{3+}, and $\chi_{obs.}$ the susceptibility observed in the Sm_3S_4 sample obtained in this study. The fraction of Sm^{3+} ion determined from the equation (16) was found as 88 %. This value agreed approximately with the value deduced from its lattice parameter (Table 6).

The solid solutions obtained by mixing Gd_3S_4 with Sm_3S_4, however, showed no van Vleck's paramagnetism. The magnetic data are summarized in table 7. Since the susceptibility of the Gd^{3+} ion present in the solid solution contributes greatly to the whole susceptibility of the solid solution, the

Table 7. Magnetic data for $(Sm_{1-x}Gd_x)_3S_4$.

Composition	θ_p (°K)	Tc (°K)	Type of conduction
$(Sm_{0.9}Gd_{0.1})_3S_4$	-34.7	-	Semiconducting
$(Sm_{0.75}Gd_{0.25})_3S_4$	-16.2	-	"
$(Sm_{0.5}Gd_{0.5})_3S_4$	-4.0	-	"
$(Sm_{0.333}Gd_{0.667})_3S_4$	-6.6	-	"
$(Sm_{0.2}Gd_{0.8})_3S_4$	-5.9	-	"
$(Sm_{0.15}Gd_{0.85})_3S_4$	+24.3	17.5	Metallic
$(Sm_{0.1}Gd_{0.9})_3S_4$	+41.0	29.0	"
Gd_3S_4	+64.8	61.2	"

estimation of the fraction of Sm^{3+} ions from the susceptibility data can not be done. The susceptibilities of the semiconducting samples obeyed the Curie-Weiss law at the range 4.2 - 300K and their paramagnetic Curie temperatures, θ_p, were all negative, while at the low temperatures the metallic materials became ferromagnets. In this system, the ferromagnetic ordering may not result from the Gd^{3+}-Sm^{2+} or Sm^{2+}-Sm^{2+}* interaction but the Gd^{3+}-Gd^{3+} interaction because Sm^{2+} is a non-magnetic ion. Apparently from the electrical properties of this system, the ferromagnetic ordering is only realized by the existence of the conduction electrons. This suggests the occurrence of the magnetic interaction of a Gd^{3+} with another Gd^{3+} via the conduction electrons. The conduction electrons, which would effectuate the magnetic interaction with the 4f spins of Gd^{3+} ions even though above the Curie

*In the metallic samples, most of Sm ions contained are divalent ions as shown in Fig. 13.

temperature, are expected to be magnetically trapped by 4f spins and their effective mass may be larger than that of the free electron [43]. In this way the magnetic polaron contributes to the increase in electrical resistivity as shown in Fig. 15.

2-4 Summary

Electrical and magnetic properties of mixed valence rare earth sulfides, $(Sm_{1-x}Gd_x)_3S_4$, were studied. The results obtained in this chapter are summarized as follows.

1. The valence transition from trivalent to divalent of Sm ions in $(Sm_{1-x}Gd_x)_3S_4$ was gradually taken place with increasing Gd concentration, and is found to be a new type of the valence transition, distinct from that observed in mixed valence samarium compounds, $Sm_{1-x}Gd_xS$.

2. The conductivity of the materials gradually decreased up to x=0.80 with increasing Gd concentration, in spite of mixing metallic Gd_3S_4 with semiconducting Sm_3S_4. A drastic change from the semiconducting to metallic conduction, however, is observed at the range between x=0.80 and x=0.85. These phenomena are explained by the valence change of the samarium ion in the solid solution, that is, the mechanism of the conduction in semiconducting materials is an electron hopping between Sm^{2+} and Sm^{3+} sites, and the mechanism in metallic materials is a band conduction through conduction electrons.

3. A maximum in the resistivity vs temperature curve for metallic samples appears near its Curie temperature. It

seems that this phenomenon is due to the formation of magnetic polarons which result from the magnetic interaction between the spins of conduction electrons and the spins of 4f electrons of Gd^{3+} ions.

Chapter 3

Electrical Properties of Ferromagnetic $Gd_{3-x}S_4$ near its Curie Temperature

3-1 Introduction

Gadolinium sulfides, $Gd_{3-x}S_4$ ($0 \leqslant x \leqslant 1/3$), crystallize in a bcc Th_3P_4 structure. These compounds possess some interesting physical properties [44-46] because of their unique crystal structure. The data of magnetic susceptibility measurements show that gadolinium contained is in a 3+ ionic state in the Th_3P_4-type sulfides. Since a sulfur atom cannot accept more than two electrons to become a sulfide anion, there are extra electrons for compositions with $x < 1/3$, and these electrons must be in a conduction band.

The conduction electrons introduced into the sample with $x < 1/3$ have a significant influence on the magnetic properties of $Gd_{3-x}S_4$ system [47]. Since the dominant magnetic interaction comes from 4f localized electrons of Gd^{3+} ions, the magnetic ordering in $Gd_{3-x}S_4$ is usually considered to be based on the f-f indirect exchange via the conduction electrons.

In this chapter, these ferromagnetic $Gd_{3-x}S_4$ compounds are chosen for the explanation of the electrical behaviors for metallic $(Sm_{1-x}Gd_x)_3S_4$ samples in the chapter 2, and their electrical and magnetic properties are investigated in detail near its Curie temperature.

3-2 Experimental

Preparation of samples

Nonstoichiometric $Gd_{3-x}S_4$ was prepared by the following two-step procedures. First, stoichiometric Gd_2S_3 was obtained by the method described in the chapter 1. For the preparation of $Gd_{3-x}S_4$, the Gd_2S_3 sample which was pressed into pellets at 200 kg/cm^2 was heated on a molybdenum plate in an induction furnace at various temperatures (1400 - 1600°C) for 3 - 6 hr in vacuum (~ 10^{-4} mmHg).

Analyses

The gadolinium content in the nonstoichiometric samples obtained was ascertained with an EDTA titration method in a neutral or weak hydrochloric medium using a xylenol orange indicator.

Some physical measurements

Some physical measurements such as X-ray diffraction, magnetic susceptibility, and electrical conductivity were made by the same methods described in foregoing chapters.

3-3 Results and discussion

Six samples were obtained for this study. X-ray powder diffraction patterns of these samples were all identical with that of the Th_3P_4 structure. In Table 8 are given the analytical values and the lattice constants for nonstoichiometric $Gd_{3-x}S_4$ samples obtained.

Temperature dependences of the electrical resistivity for

Table 8. Compositions and lattice constants for $Gd_{3-x}S_4$.

Sample No.	Firing schedule (°C)	(hr)	Composition x	Lattice constant (A)
1	1400	3	0.34 ± 0.01	8.387
2	1500	3	0.29 ± 0.01	8.379
3	1550	3	0.29 ± 0.01	8.377
4	1550	3	0.28 ± 0.01	8.380
5	1600	4	0.26 ± 0.01	8.381
6	1600	6	0.25 ± 0.01	8.379

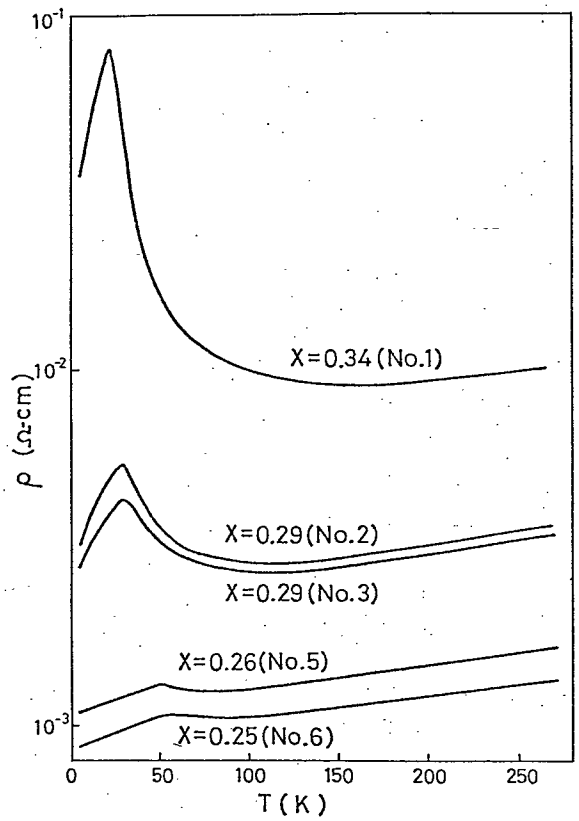

Fig. 19. Temperature dependence of electrical resistivity for a series of $Gd_{3-x}S_4$.

a series of $Gd_{3-x}S_4$ are shown in Fig. 19. At high temperature all samples indicate a common metallic behavior, that is, the resistivity linearly increases with the rise of temperature. A maximum in resistivity is, however, observed in the curve of resistivity vs temperature for all cases at low temperature. The maximum increases in height and shifts to low temperature side as x increases.

The magnetic data were obtained in the temperature range 4.2 - 300K. The magnetic susceptibilities for all samples obeyed the Curie Weiss law. Paramagnetic Curie temperatures, θ_p, are listed in Table 9. The sign of θ_p for all samples is

Table 9. Magnetic and electrical data.

Sample No.	θ_p (°K)	T_c (°K)	T_p (°K)	ρ_{max} ($\times 10^{-3}\Omega$cm)	ρ_p ($\times 10^{-3}\Omega$cm)	$\Delta\rho$ ($\times 10^{-3}\Omega$cm)
1	24	-	21.0	81.81	7.238	74.57
2	32	-	28.5	5.378	2.023	3.364
3	36	-	30.2	4.346	1.947	2.399
4	36	-	31.5	4.688	2.349	2.339
5	56	51.0	51.0	1.297	1.075	0.222
6	62	-	55.0	1.609	0.902	0.149

positive, indicating a ferromagnetic behavior. The values of θ_p are approximately in agreement with the values of temperatures, T_p, at which the resistivity maxima emerge. For $Gd_{2.74}S_4$ (No. 5) the dependences of the magnetization I on the magnetic field H and on the temperature near θ_p were investigated. The results obtained are shown in Fig. 20. The relationship of I vs H below 50K is typical of ferromagnetic

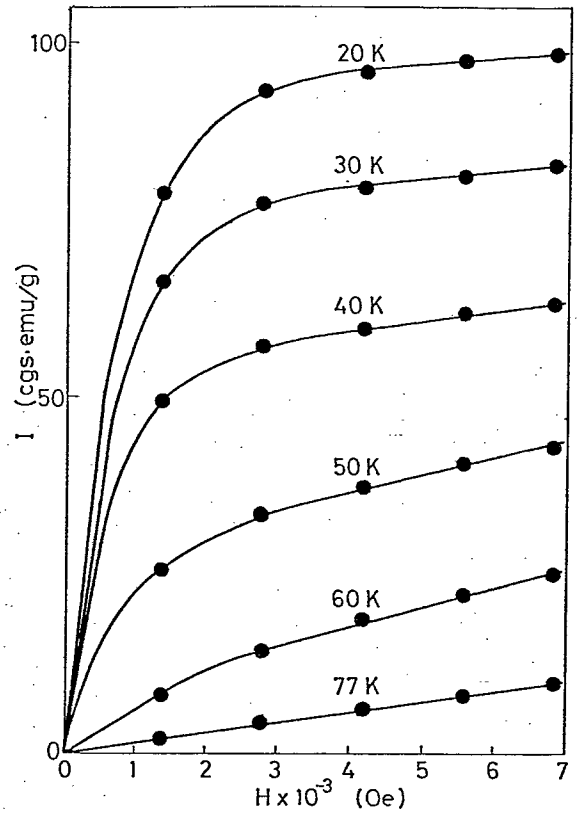

Fig. 20. Magnetic field dependence of magnetization for $Gd_{2.74}S_4$ (No. 5) at various temperatures.

characteristics. The Curie temperature T_c for this sample was determined, using the method proposed by Arrott et al. [48]. As a result, the obtained Curie temperature, 51K, coincides with its T_p.

The maxima in resistivity as shown in Fig. 19 are similar to that observed in ferromagnetic $Eu_{1-x}Gd_xS$ system [35,49,50], where the indirect exchange via conduction electrons occurs between localized 4f spins, leading to the formation of magnetic polarons. There have been no quantitative expla-

nations for this phenomenon in these eariler studies. Here, the height and position of the resistivity maximum observed in the resistivity vs temperature curve are quantitatively treated on the basis of the concept of magnetic polaron.

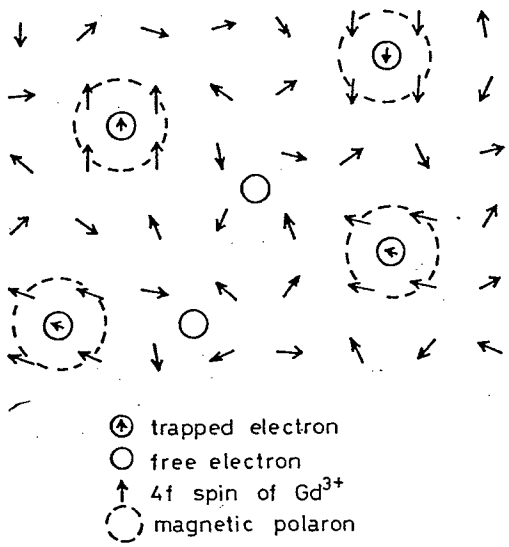

Fig. 21. Scheme of electrons trapped by 4f spins and free electrons.

First, it assumes for metallic $Gd_{3-x}S_4$ that two type of electrons exist in the conduction band with lowering temperature as schematically described in Fig. 21. One type of electrons is magnetically trapped with 4f spins of Gd^{3+} ions and form a new localized state below the conduction band. The other is magnetically "free" electrons. If the mobility of the trapped electrons is negligibly small compared with that of the free electrons, the reciprocal value of the number of the free electrons should be in proportion to the resistivity of the sample at a constant temperature. When the number of conduction electrons present in the sample is denoted by n_c, the number of the free electrons at low temperatures can be denoted by $n_c - n_m$, where n_m expresses the number of the trapped electrons. According to the Boltzmann distribution law, the ratio of the number of the

oscillators N_1 in the upper energy state to the number N_2 in the lower energy state is given in the thermal equilibrium by the Boltzmann factor k

$$\frac{N_1}{N_2} = \exp(-E/kT), \tag{17}$$

where E is an energy difference between two states. Thus, in the system under consideration, one easily obtains

$$\frac{n_c - n_m}{n_m} = \exp(-E/kT). \tag{18}$$

In this study, the values of log $(\Delta\rho/\rho_p)$ are plotted as a function of the reciprocal values of T_p in Fig. 22. The value of the ρ_p can be regarded as the resistivity value in the case where no magnetic interaction exist between conduction electrons and 4f spins of Gd^{3+}. The following relation can be derived from the definition of the

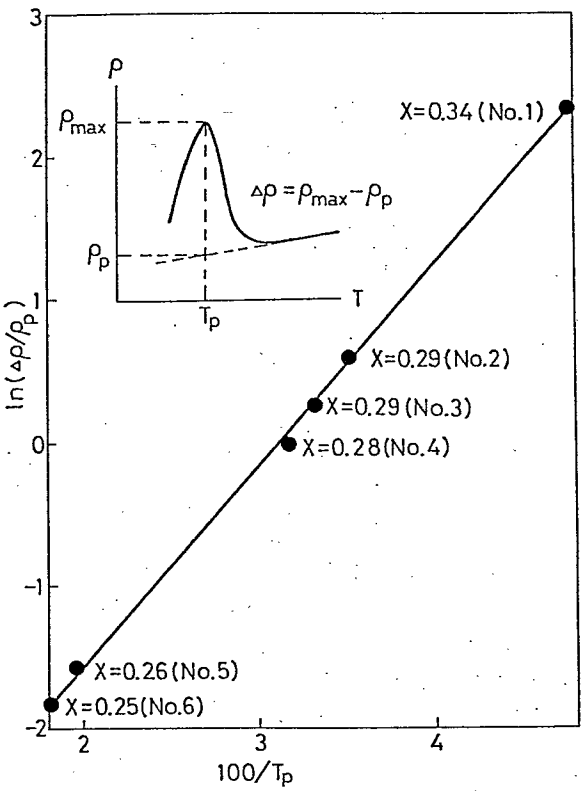

Fig. 22. Log $(\Delta\rho/\rho_p)$ vs reciprocal of T_p, insert; example for temperature dependence of ρ.

electrical resistivity in solids.

$$\rho_{max} \propto \frac{1}{n_c - n_m}, \tag{19}$$

$$\rho_p \propto \frac{1}{n_c}. \tag{20}$$

Then, one obtains

$$\Delta\rho/\rho_p = (\rho_{max} - \rho_p)/\rho_p \propto \frac{n_m}{n_c - n_m}. \tag{21}$$

Thus, the value of $\Delta\rho/\rho_p$ gives the ratio of the number of the trapped electrons n_m to the number of the free electrons $(n_c - n_m)$. As is shown in Fig. 22, the linearity is obtained in the plot of log $(\Delta\rho/\rho_p)$ and $1/T_p$, and means the relationship

$$\Delta\rho/\rho_p \left(\propto \frac{n_m}{n_c - n_m}\right) \propto \exp(E_a/kT). \tag{22}$$

The equation (22), which is derived from the experimental results, is the same as the equation (18) derived from the dual-type ("free" and "trapped") electrons model. The value, E_a, in the equation (22) is 0.012 eV. This energy is thiught to be the energy gap between the state of trapped and free

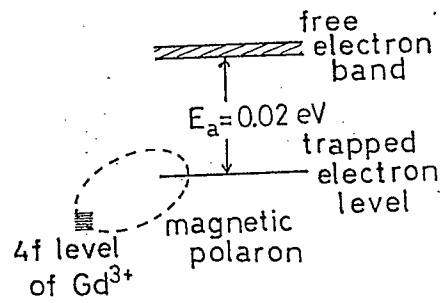

Fig. 23. Band model for $Gd_{3-x}S_4$ near T_c.

electrons as shown in Fig. 23, and seems to relate to an exchange interaction.

At temperatures below the Curie temperature, T_p, the magnetic polarons would disappear because most of the 4f spins of Gd^{3+} ions order ferromagnetically. The state of the trapped electrons may be no longer localized.

3-4 Summary

Nonstoichiometric $Gd_{3-x}S_4$ $(0 < x < 1/3)$, which exhibited a metallic behavior, was obtained by heating an insulating Gd_2S_3 at various temperatures under a high vacuum. Electrical and magnetic properties of the samples obtained have been investigated from 4.2 to 300K. A maximum in resistivity is observed in the curve of resistivity vs temperature. The temperature, T_p, at which the maximum emerges, is very close to the Curie temperature, T_c, for the sample. An increase in resistivity at T_p, $\Delta\rho$, is proportional to $\rho_p \exp(E_a/kT)$, where ρ_p is the resistivity obtained by the extrapolation from the linear portion to T_p in the ρ vs T curve. Using the relationship obtained, a dual-type ("free" and "trapped") electrons model is proposed for this system on the basis of the formation of magnetic polarons.

Chapter 4

Concluding remarks

In the work of this thesis, electrical properties of various rare earth sulfides were investigated for the purpose of developing new effective semiconductors. The main conclusions to be drawn from this work are as follows.

1. $EuLn_2S_4$ (Ln = La - Gd) compounds are all p-type semiconductors. This finding represents relatively unusual behaviors among Th_3P_4-type materials, most of which are metallic or n-type semiconducting materials. The origin of the p-type behavior is found to be positive holes produced in the following equilibrium reaction;

$$1/2\ S_2 \rightleftharpoons S_S + V_{Eu}'' + 2\ h^{\bullet}$$

2. The samples obtained from heating stoichiometric $EuGd_2S_4$ under a high vacuum and high temperatures are classified into semiconducting and metallic materials. The electrical transport mechanism for semiconducting materials is found to be via electron hopping between localized states resulting from the fluctuating random field, which is produced by the sublimation of Eu and S components. Metallic materials exhibit a band conduction.

3. In mixed valence rare earth sulfides, $(Sm_{1-x}Gd_x)_3S_4$, a drastic change from semiconducting to metallic conductions is observed at the range between x = 0.80 and x = 0.85.

This phenomenon is explained by the assumptions that the conduction mechanism for semiconducting samples is an electron hopping between Sm^{2+} and Sm^{3+} sites, and that the mechanism for metallic samples a band conduction through conduction electrons.

4. A resistivity maximum which corresponds to the magnetic ordering between Gd^{3+} ions is observed in the resistivity vs temperature curves for ferromagnetic $(Sm_{1-x}Gd_x)_3S_4$ and $Gd_{3-x}S_4$. From the results of quantitative treatment for their electrical behaviors, dual-type ("free" and "trapped") electrons model is proposed for this phenomenon on the basis of the formation of magnetic polarons.

Acknowledgement

This work was supervised by Professor Dr. Jiro Shiokawa, to whom the author is deeply indebted for his invaluable guidance and continous encouragement through out this work.

The author is also very much obliged to Associate Professor Dr. Gin-ya Adachi for his numerous fruitful discussions and helpful suggestions in the course of this thesis and for kindful suggestions to prepare the manuscripts.

The author is very grateful to Mr. Yoshiyuki Hirashima, Dr. Tsuyoshi Arakawa, and Dr. Tsutomu Shin-ike for their encouragement and helpful advices.

Thanks are given to the author's co-workers, Mr. Ken-ichi Niki and Mr. Nobuhito Imanaka for their assistances, and all the members of Shiokawa group and all my friends for their friendships.

Finally, the author wishes to thank Professor Dr. Masakazu Sakaguchi of Niigata University for his kindly support of this research.

References

1. H. P. Leppin, D. K. Wohlleben, and B. C. Sales, Physica, 86-88B&C, 241(1977).
2. S. von Molnar and S. Methfessel, J. Appl. Phys., 38, 959(1967).
3. R. Didchenko and F. P. Gortsema, J. Phys. Chem. Solids, 24, 863(1963).
4. M. Cutler and J. F. Leavy, Phys. Rev., 133, A1153(1964).
5. T. Kasuya and Yanase, Rev. Mod. Phys., 40, 684(1968).
6. S. M. A. Taher, J. B. Gruber, and L. Olsen, J. Chem. Phys., 60, 2050(1974).
7. A. Jayaraman, P. Dernier, and L. D. Longinotti, Phys. Rev., B11, 2783(1975).
8. K. Meisel, Z. Anorg. Allgem. Chem., 240, 300(1939).
9. P. L. Kripyakevich, Soviet Phys.-Cryst., 7, 556(1963).
10. M. Cutler, R. L. Fitzpatrick, and J. F. Leavy, J. Pgys. Chem. Solids, 24, 319(1963).
11. O. A. Golikova, I. M. Rudnik, V. Sergeva, M. M. Kazanin, and E. N. Tkalenko, Phys. Status Solidi (a), 37, 199(1976).
12. M. Cutler and N. F. Mott, Phys. Rev., 181, 1336(1969).
13. V. Tien, J. Flahaut, and L. Domange, C. R. Acad. Sci. Paris, 262, 278(1966).
14. W. Lugscheider, H. Pink, K. Weber, and W. Zinn, Z. Angew. Physik., 30, 36(1970).
15. P. Wachter, Z. Angew. Physik., 32, 171(1971).
16. J. F. Miller, L. K. Matson, and R. C. Himes, "Rare Earth Research" (K. S. Vorres, Ed.), Vol.II, p.135, Gordon & Breach, New York (1963).
17. A. Jayaraman, E. Bucher, P. D. Dernier, and L. D. Longinotti, Phys. Rev. Lett., 31, 700(1973).
18. A. Jayaraman, V. Narayanamurti, E. Bucher, and R. G. Maines,

Phys. Rev. Lett., 25, 1430(1970).

19. A. Menth, E. Buehler, and T. H. Geballe, Phys. Rev. Lett., 22, 295(1969).

20. J. C. Nickerson, R. M. White, K. N. Lee, R. Buchmann, T. H. Geballe, and G. W. Hull Jr., Phys. Rev., B3, 2030(1971).

21. W. H. Zachariasen, Acta Cryst., 2, 57(1949).

22. F. L. Cater, J. Solid State Chem., 5, 300(1972).

23. M. Eibschütz, R. L. Cohen, E. Buehler, and J. H. Wernik, Phys. Rev., B6, 18(1972).

24. O. Berkooz, M. Malamud, and S. Shtrickman, Solid State Comm., 6, 185(1968).

25. B. Batlogg, E. Kaldis, A. Schlegel, G. von Schulthess, and P. Wachter, Solid State Comm., 19, 673(1976).

26. A. I. Smirnov, L. S. Parfen'evea, V. Ya Khusmut, and V. M. Sergeeva, Fiz. Tverd. Tera, 14, 2783(1972).

27. M. Ohashi, T. Kaneko, H. Yoshida, and S. Abe, Physica, 86-88 B&C, 224(1977).

28. B. Batlogg, E. Kaldis, and P. Wachter, J. Mag. Mag. Mat., 3, 96(1976).

29. J. M. D. Coey, S. K. Ghatak, M. Avignon, and F. Holtzberg, Phys. Rev., B14, 3744(1976).

30. M. Avignon, S. K. Ghatak, and J. M. D. Coey, J. Mag. Mag. Mat., 3, 88(1976).

31. J. N. Chazalviel, M. Campagna, G. K. Wertheim, P. H. Smith, and Y. Yafet, Phys. Rev. Lett., 37, 919(1976).

32. R. L. Cohen, M. Eibschütz, and K. W. West, Phys. Rev. lett., 24, 383(1970).

33. R. D. Shannon, Acta Cryst., A32, 75(1976).

34. M. Campagna, E. Bucher, G. K. Wertheim, and L. D. Longinotti, Phys. Rev. Lett., 33, 165(1974).

35. Y. Shapira and T. B. Reed, Phys. Rev., B5, 4788(1972).

36. T. Kasuya, A. Yanase, and T. Takeda, Solid State Comm., 8, 1543(1970).

37. E. Kaldis and P. Wachter, Solid State Comm., 11, 907(1972).

38. E. Kaldis, A. Schlegel, P. Wachter, and Ch. Zurder, J. Mag. Mag. Mat., 3, 1(1976).

39. V. P. Zhuze, A. A. Kamarzin, M. G. Karin, K. K. Sidorin, and A. I. Shelykh, Fiz. Tverd. Tela, 21, 3401(1979).

40. J. M. Robinson, Phsy. Rep., 51, 1(1979).

41. E. Bucher, V. Narayanamurti, and A. Jayaraman, J. Appl. Phys., 42, 1741(1971).

42. M. Escorne, A. Ghazali, P. Lerouxhugon, and I. A. Smirnov, Phys. Lett., 56A, 475(1976).

43. S. von Molnar and S. Methfessel, J. Appl. Phys., 38, 959 (1967).

44. V. I. Marchenko, Poluchenie i issled. svoistv. RZM, 51(1975).

45. S. M. A. Taher, John B. Gruber, and L. C. Olsen, J. Chem. Phys., 60, 2050(1974).

46. J. R. Henderson, M. Muramoto, E. Loh, and John B. Gruber, J. Chem. Phys., 47, 3347(1967).

47. D. G. Andrianov, G. P. Borodulenko, A. A. Grzik, S. A. Drozdov, and V. I. Fistul', Fiz. Tverd. Tela, 17, 1831(1975).

48. A. Arrott and J. Noakes, Phys. Rev. Lett., 19, 786(1967).

49. S. von Molnar, IBM J. Res. Developm., 14, 269(1970).

50. P. Wachter, CRC Crit, Rev. Solid State Science, 3, 189(1972).